COMPETING BROADBAND NOISE MECHANISMS OF A GENERIC LOW-SPEED AXIAL FAN INCLUDING ACOUSTIC SCATTERING

Korcan KUCUKCOSKUN, Julien CHRISTOPHE,
Christophe SCHRAM

von Karman Institute for Fluid Dynamics, Aeroacoustic Research Unit,
72 Chaussée de Waterloo. 1640 Rhode–St–Genèse, Belgium

SUMMARY

This paper focuses on the semi-analytical modeling of the broadband noise generated by a low-speed axial fan and of its scattering by an obstacle. Two different broadband noise mechanisms are investigated: leading-edge noise and trailing-edge noise. The theories of Amiet on turbulence-interaction noise and trailing-edge noise are employed including a geometrical near-field extension. The scattering of the broadband noise of the axial fan is taken into account by means of the Acoustic Transfer Vector (ATV) method implemented in a Boundary Element Method (BEM) commercial solver. A good agreement is obtained with an analytical solution obtained for the scattering by a flat screen assumed to be infinite, using the method of images.

INTRODUCTION

The reduction of broadband noise for axial fans remains a challenging task as it contributes equally with tonal noise to the total sound radiated in numerous configurations [1,2]. The contribution of broadband noise includes several competing mechanisms. On the one side, trailing-edge noise, caused by the scattering of boundary-layer pressure fluctuations into acoustic waves at the blade trailing edge, always exists and represents the minimum noise that a fan would produce in absence of any interaction [3]. On the other side, turbulence interaction noise, due to flow disturbances impacting blade leading edges, is present in most of the applications, as in cooling automotive modules when a heat exchanger is located upstream of the fan for example [1]. The present paper proposes to address the importance of both sound mechanisms on the total sound production, and their respective variation with the upstream turbulence flow properties. The proposed method is based on Amiet's thin airfoil theory [4,5], combined in this work with Reynolds-Averaged Navier-Stokes (RANS) computations to obtain the required turbulence model scaling data.

Another point addressed in this paper is the scattering of different broadband acoustic sources. As the fan is usually operating in presence of surrounding surfaces, the acoustic free-field assumption becomes questionable. Hence the scattering due to the installation effects must be accounted for.

Helmholtz solvers [6] and Linearized Euler Equation (LEE) [7] solvers are already widely used in industry accounting for acoustic scattering due to installation effects. The Equivalent Source Method (ESM) [8] has also been recently used for exterior scattering problems. However they all require a deterministic description of the source field (or at least acoustic near-field), while in Amiet's theory the incident acoustic field is given in statistical sense, relying on statistical descriptions of the incident turbulent velocity or wall pressure fields. Therefore, Amiet's theory is combined with the Acoustic Transfer Vector (ATV) [9,10] methodology of BEM framework to overcome the lack of deterministic source field description. This approach is applied to both leading-edge and trailing-edge noise models for a stationary airfoil and a generic axial fan operating next to a flat scattering screen.

NOISE PREDICTION METHODS

In the present paper, both broadband leading-edge and trailing-edge noise mechanisms are investigated. The noise prediction methods for both mechanisms are based on corresponding Amiet's theory for turbulence-interaction noise and trailing-edge noise, solving iteratively scattering problems at airfoil edges. It assumes the airfoil to be infinitively thin, without camber or angle of attack, and in uniform flow conditions. The main leading/trailing-edge scattering obtained by Amiet [4,5] has been corrected by a trailing/leading-edge back-scattering contribution which fully accounts for the finite chord length [11,12]. The radiated sound field is calculated by integrating the induced surface sources on the actual chord length C, and the airfoil span L, assuming convection of frozen turbulence upstream of the leading edge or past the trailing edge. For large airfoil aspect ratio (L/C), the Power Spectral Density (PSD) of the sound pressure in the geometrical far field is obtained for both noise mechanisms using

$$S_{pp}(\boldsymbol{x},\omega) = \left(\frac{\rho_0 kzb}{\sigma_0^2}\right)^2 \pi U d \left|\mathcal{L}\left(\boldsymbol{x},K_x,K_y\right)\right|^2 \Phi_{ww}\left(K_x,K_y\right) \tag{1}$$

for leading-edge noise, or

$$S_{pp}(\boldsymbol{x},\omega) = \left(\frac{kzb}{\pi\sigma_0^2}\right)^2 d \left|\mathcal{L}\left(\boldsymbol{x},K_x,K_y\right)\right|^2 \Phi_{pp}(\omega) l_y\left(K_y,\omega\right) \tag{2}$$

for trailing-edge noise, where $\mathbf{x}=(x,y,z)$ is the observer position, b and d are the airfoil half-chord and span respectively, ρ_0 is the fluid density, $k=\omega/c_0$ is the wavenumber, with ω the angular frequency and c_0 the speed of sound. σ_0 is the airfoil-listener distance corrected for convection effects. K_x and K_y are gust wavenumbers defined as $K_y=k_y/\sigma_0$, and $K_x= \omega/U$ or $K_x= \omega/U_c$ for leading-edge or trailing-edge theories respectively, where U is the flow velocity upstream of the leading edge and U_c is the convection velocity past the trailing-edge. $\mathcal{L} = \mathcal{L}_1 + \mathcal{L}_2$ is the aeroacoustic transfer function, derived analytically, with $\mathcal{L}_1$ the main contributing term from the leading/trailing-edge [4,5] and $\mathcal{L}_2$ the back-scattering term from the trailing/leading-edge [11,12], for leading and trailing-edge noise theories respectively. In case of scattering of noise by surrounding surfaces, the formulations (1) and (2) can be extended to take into account observers that are located in the geometrical near-field. Such an extension has been published previously for the leading-edge noise prediction [9,13] and is developed in the present work for trailing-edge formulation, similarly to previous work in literature [14].

In case of leading-edge noise formulation, the main flow input is the upwash turbulence spectrum Φ_{ww} upstream of the leading edge. In the present work, the von Karman spectrum is used and defined as [4]:

$$\Phi_{ww}\left(k_x,k_y\right) = \frac{4}{9\pi}\frac{\overline{u^2}}{k_e^2}\frac{\hat{k}_x^2+\hat{k}_y^2}{\left(1+\hat{k}_x^2+\hat{k}_y^2\right)^{7/3}} \tag{3}$$

where $\widehat{k_\iota}$ are the wave-numbers made non-dimensional by $k_e = (\sqrt{\pi}/\Lambda)\Gamma(5/6)\Gamma(1/3)$. The flow relevant parameters are then the RMS of the squared axial velocity fluctuations $\overline{u^2}$ and the integral length scale of turbulence Λ.

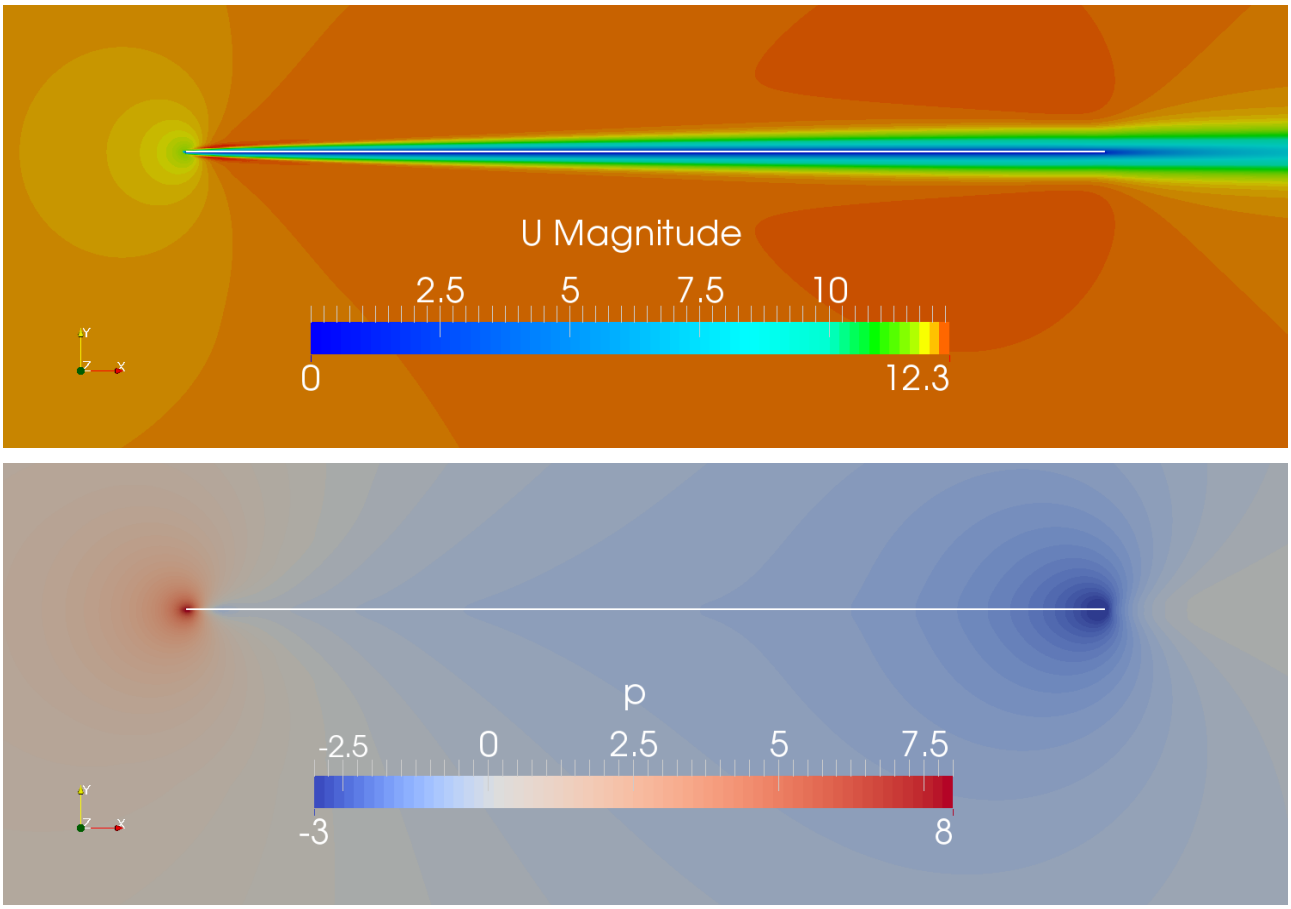

Figure 1: Contours of (top) velocity magnitude and (bottom) pressure. T.I. = 0.025, Λ = 0.05 m.

For the trailing-edge noise formulation, the trailing-edge wall pressure spectrum Φ_{pp} is computed using Panton and Linebarger's reconstruction method [15,16]. The model uses the streamwise mean velocity profile and the crosswise velocity fluctuation profile near the trailing edge, together with the integral length scale Λ through the boundary layer. Boundary layer profile data are then used in a quintuple integral solved with a Monte Carlo method using importance sampling to retrieve the wall pressure spectra. Further information about the method can be found in [16]. The spanwise correlation length l_y is described by Corcos' model [17].

In the present paper, the required inputs for both leading- and trailing edge noise models will be provided from 2D incompressible RANS CFD computations over a flat plate obtained using OpenFOAM. The same airfoil chord and flow conditions are later used in case of a stationary airfoil and plane scattering as well as in the fan application. A stationary, infinitively thin airfoil with 0.04 m chord (C) is placed in a uniform flow with mean velocity U=12 m/s. The computational domain is extended 3C upstream the airfoil, 6C in crosswise direction and 4C downstream. The total number of cells is 810.000 and the mesh is refined perpendicularly to the airfoil surface to reach $y^+ < 1$. The computations are performed using a k-ω SST turbulence model and second order accuracy discretisation schemes for all variables. The equations are solved till a convergence of 10^{-10} on the residuals is reached. Velocity, turbulence intensity and mixing length are imposed at the inlet, symmetry boundary conditions are used on the bottom and top boundary condition and zero pressure is imposed at the outlet. An example of the flow field around the flat plate airfoil is show in Figure 1.

The automatic extraction of data required for Amiet's theory as well as noise predictions are performed within the BATMAN (Broadband and Tonal Models for Airfoil Noise) platform, developed by VKI. The necessary flow data for trailing-edge noise prediction are extracted 5% *C* upstream of the leading edge while the boundary layer data, required for trailing-edge noise prediction, are extracted 2% *C* upstream of the trailing edge. Tests have been conducted to estimate the sensitivity of the acoustic results with respect to the extraction location, showing little influence.

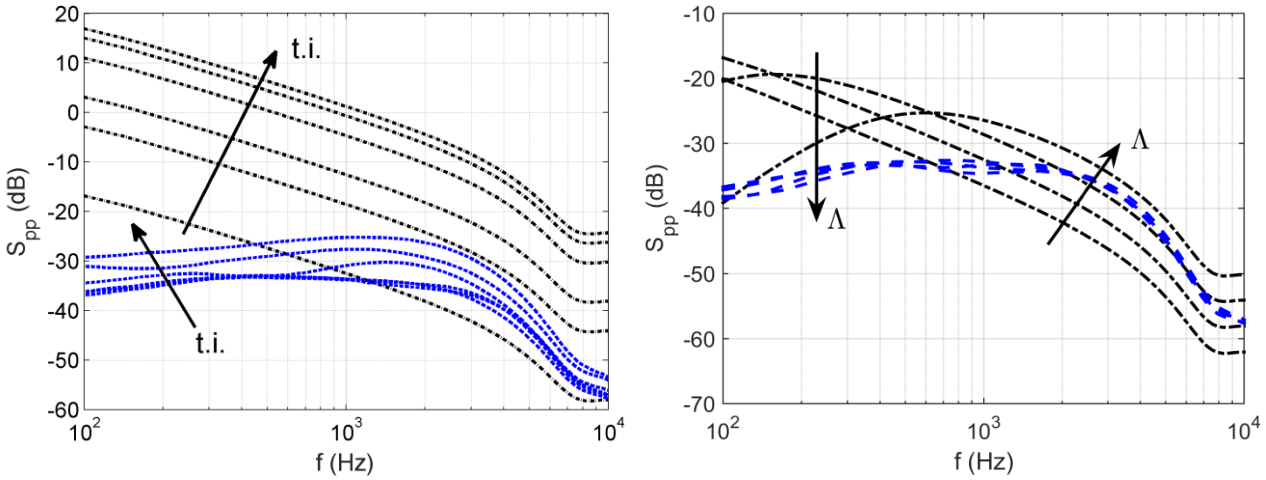

Figure 2: (Left) Influence of upstream turbulence intensity on the leading-edge (black - dash-dot) and trailing-edge noise predictions (blue - dash). T.I = [0.002, 0.009, 0.02, 0.04, 0.07, 0.08], Λ = 0.05 m. (Right) Influence of the upstream integral length scale on the sound predictions. T.I. = 0.002, Λ = [0.0031, 0.0125, 0.05, 0.2] m.

COMPETING BROADBAND NOISE MECHANISMS

Sound predictions are first made in free field in order to evaluate the importance of leading and trailing-edge noise mechanisms on the total noise predictions. Those predictions are performed using a large span airfoil of 100*C* span and an observer placed at 500*C* perpendicularly to the airfoil surface in the mid-span plane, in order to respect far-field approximations.

Different turbulence intensities and length scales are first imposed at the inlet boundary condition for the computational domain in order to estimate the influence of the turbulent flow parameters on the leading and trailing-edge sound predictions. The upstream turbulence parameters (T.I. and length scale Λ) reported below are those extracted upstream of the airfoil and are slightly different than those imposed at the inlet condition due to convection of slowly decaying turbulence from inlet to airfoil location. The influence of turbulence intensity on the leading and trailing-edge predictions are shown in Figure 2 (left), for fixed turbulence integral length scale. As expected, the turbulence intensity only affects the amplitude of the leading-edge sound spectrum as it only involved as a scaling factor in the upstream turbulence spectrum. The trailing-edge sound spectrum is not altered by the upstream conditions as long as the turbulence intensity remains below 1%. For higher values, an increase of the trailing-edge radiated sound spectra is observed with the amplitude of the impacting turbulence intensity. For such values, the boundary-layer development starting from the leading edge is affected, resulting in a different wall-pressure spectrum upstream of the trailing-edge.

The influence of the turbulence integral length scale on the sound predictions is shown in Figure 2 (right) for fixed turbulence intensity. As the upstream turbulence spectrum energy is fixed by the turbulence intensity, the length scale has an influence on the spectrum shape only. The increase of the length scale results in a decrease of the turbulence flow spectrum amplitude at low frequencies, accompanied by an increase at high frequencies. The changes in the upstream flow spectrum are directly transposed to the leading-edge sound predictions. Unlike the turbulence intensity

observations, the trailing-edge predictions are not influenced by the variation of the length scale in the tested range of parameters.

The turbulence intensity and integral length scale are selected as 0.2 % and 0.05 m respectively, in order to have both leading and trailing-edge contributions participating to the radiated sound. These values will be used for all results presented below, including for the predictions including sound scattering effects. The inputs spectra used for leading and trailing-edge Amiet formulations are shown in Figure 3 (left) and the corresponding sound predictions are shown in Figure 3 (right) with

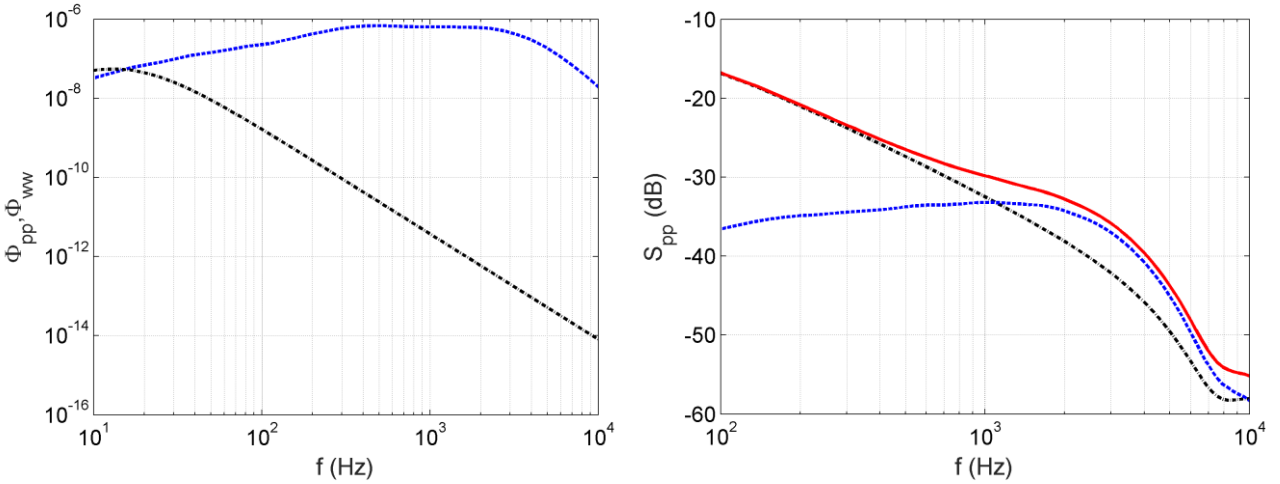

Figure 3: (Left) Input spectra for leading-edge (black – dash-dot) and trailing-edge (blue - dash) Amiet's formulations. (Right) Total radiated sound (red - plain) from leading-edge (black – dash-dot) and trailing-edge (blue - dash) contributions computed using Amiet's theory. T.I. = 0.002, Λ = 0.05 m.

the total sound spectrum obtained by summing both contributions. With the selected upstream turbulence parameters, the leading-edge contribution is dominating the total sound radiated for low frequencies below 1 kHz. Around 1 kHz, both noise mechanisms have similar amplitudes. Above that frequency, the trailing-edge sound radiation presents higher values the leading edge one, both having again similar amplitudes around 10 kHz.

Directivities of the normalized radiated sound for both noise mechanisms are shown in *Figure **4***, for particular frequencies and observers located in the mid-span plane. At the low frequency of 500 Hz (kC = 0.37), the leading-edge sound is higher for all radiation angles while both sound mechanisms have similar amplitudes at 1 kHz (kC = 0.74). For both frequencies, a low frequency compact dipole pattern is observed. Increasing frequency to 5 kHz (kC = 3.7), the directivity lobes are tilted towards the downstream or upstream directions for leading and trailing-edge noise respectively, as observed previously in literature [1]. At that frequency, the trailing-edge sound radiation is larger for all radiation angles compared to leading-edge sound except for small downstream radiation angles. At high frequency (kC = 7.4), both sound mechanisms have similar amplitudes and both contribute in a similar manner to the total sound, with similar directivities, radiating upstream for trailing-edge noise and downstream for leading-edge noise.

BROADBAND SCATTERING

This paper also deals with the scattering of the noise of different broadband mechanisms such as leading-edge and trailing-edge noise. Analytical scattering techniques are mostly limited with simplified scattering obstacles. Numerical acoustic techniques - such as BEM and FEM - usually require a deterministic description of the incident field on the scattering surface [6], i.e. including amplitude and phase. However the leading-edge and trailing-edge models described above provide only a statistical description of the incident sound field, related to statistical models for the turbulence approaching the leading edge (e.g. the von Karman spectrum) or the incoming pressure

field approaching the trailing edge (e.g. the Corcos model). In previous works, the present authors proposed an application of the Acoustic Transfer Vector methodology implemented in a Boundary Element Method solver, to predict the scattering of leading edge noise obtained using Amiet's statistical model, for a steady airfoil and a low-speed fan [9,13]. This approach is here extended to the prediction of trailing edge noise, also based on Amiet's approach.

The total acoustic field is first decomposed into incident (free)-field and scattered field pressure, $p = p_i + p_s$. The scattered field pressure is linked to the wall-normal velocities $\{v_n(\omega)\}$ as follows:

$$p_s(\omega) = \{\mathbf{ATV}(\omega)\} \cdot \{v_n(\omega)\}. \quad (4)$$

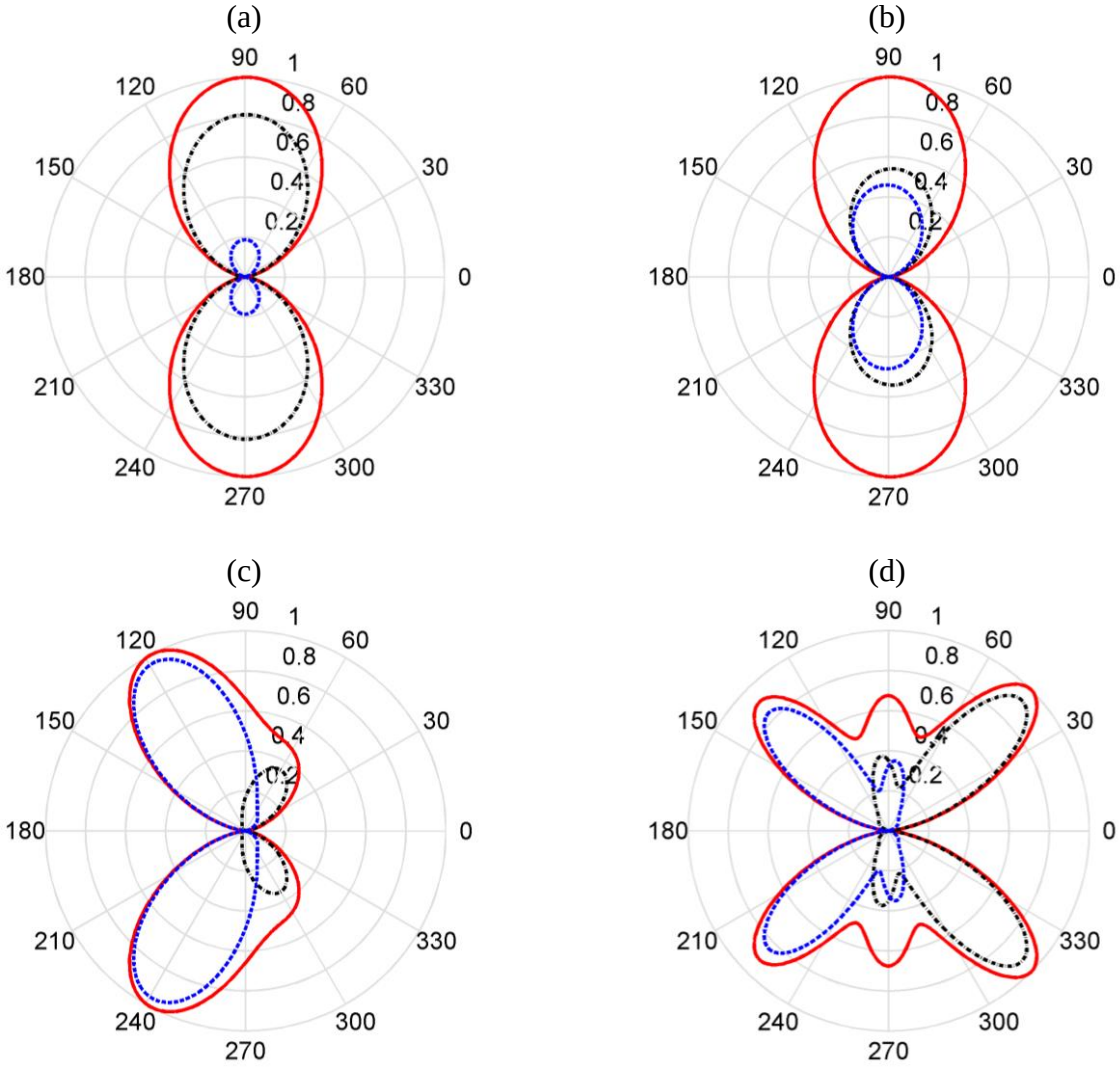

Figure 4: Normalized total radiated sound (red - plain) and contributions from leading-edge (black – dash-dot) and trailing-edge (blue - dash) in the airfoil mid-span plane. (a) 500 Hz, (b) 1 kHz, (c) 5 kHz and (d) 10 kHz.

Since the summation of the scattered and incident field will be zero satisfying the rigid Neumann boundary condition on the scattering surface [6], the wall-normal velocities correspond to minus the incident velocity field on the acoustic mesh. The incident velocity $\{v_i(\omega)\}$ can be computed by the gradient of the incident pressure field. Finally the total PSD is computed via [9]

$$Spp_t = Spp_i - Spv \cdot \mathbf{ATV}^{\boldsymbol{T}} - \mathbf{ATV}^{*} \cdot Svp + \mathbf{ATV}^{*} \cdot Svv \cdot \mathbf{ATV}^{\boldsymbol{T}}. \quad (5)$$

Spp_i is the incident (free-field) PSD at the listener point. Svv is the auto- and cross-power spectrum of the acoustic velocities on the discretised scattering surface. Spv and Svp are then the cross-power spectra of the velocity on the scattering surface and acoustic pressure at the observer. The superscripts * and ^{T} represent the complex conjugate and transpose operators, respectively. $\mathbf{ATV}(\omega)$ is the matrix linking the pressure at the observer and velocity on the acoustic nodes. The acoustic

transfer vectors **ATV**(ω) are computed using the LMS/Siemens software Virtual.Lab and Sysnoise for each frequency of interest [6].

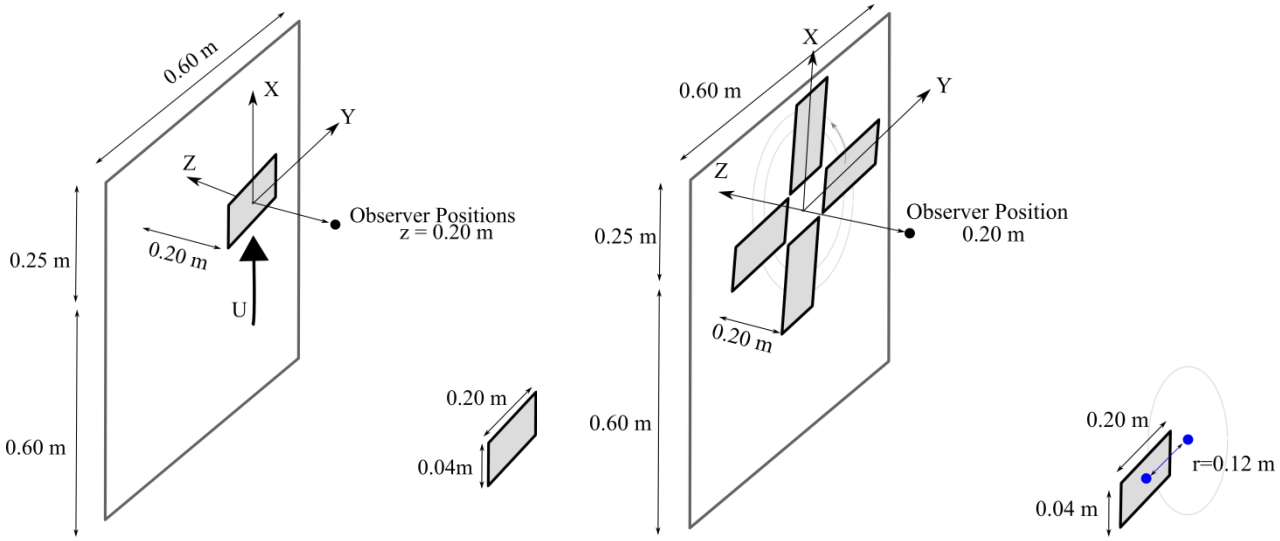

Figure 5: Sketch of the stationary airfoil (left) and generic axial-fan (right) operating in the vicinity of a scattering obstacle.

VALIDATION OF BROADBAND SCATTERING

A stationary airfoil subjected to an incoming flow field with low turbulence level is first investigated. The methodology is later applied to a low-speed fan noise problem in a similar flow-field. In this paper addressing the competition between different broadband noise sources, the dimensions and flow properties in the CFD simulations are selected in order to have both noise sources dominating different frequency ranges of the acoustic spectra.

A stationary airfoil with 0.20 m span and 0.04 m chord is considered. The airfoil geometry is selected as flat-plate as performed in the CFD simulations. The observer is located at 0.20 m away from the center of the airfoil, on the *z*-axis. Since the observer-airfoil distance is equal to the span length of the airfoil, the spanwise geometrical near-field correction proposed in reference [9] is used. The flow is assumed to be uniform on the spanwise direction. The incoming flow speed is selected as 12 m/s. The turbulence intensity and the length scale are extracted from CFD simulations, equal to 0.17% and 0.05 m for the leading-edge noise predictions. For the trailing-edge noise prediction, the wall-pressure reconstructed spectrum shown in Figure 3 (left) is used as input to the Amiet's theory.

For the scattered-field predictions, a flat screen similar to the one used in reference [9] is introduced. The dimensions of the screen are 0.60 m in the spanwise direction and 0.85 m in the streamwise direction. The distance of the screen to the airfoil is 0.20 m. A sketch of the validation case is shown in Figure 5 (left). The method proposed in the current paper is applicable to arbitrary geometries. However, a flat screen is selected as a validation case, since it is possible to solve a similar scattering problem by means of image sources assuming an infinite flat screen. (left) shows the incident (free)-field acoustic spectra in absence of the scattering screen for leading-edge, trailing-edge and their combination in black, blue and red, respectively. It is seen that, for the selected CFD output, the leading-edge noise is dominating the acoustic spectra for low-frequencies where as the trailing-edge noise is more dominant for high frequencies. The total PSD is obtained via superposition of both noise sources, assuming the leading-edge and trailing-edge noise sources are uncorrelated. It is seen that for the considered flow-field, the selection of one noise source

mechanism only can alter the complete acoustic spectrum, hence it may be necessary to consider both noise sources for such applications.

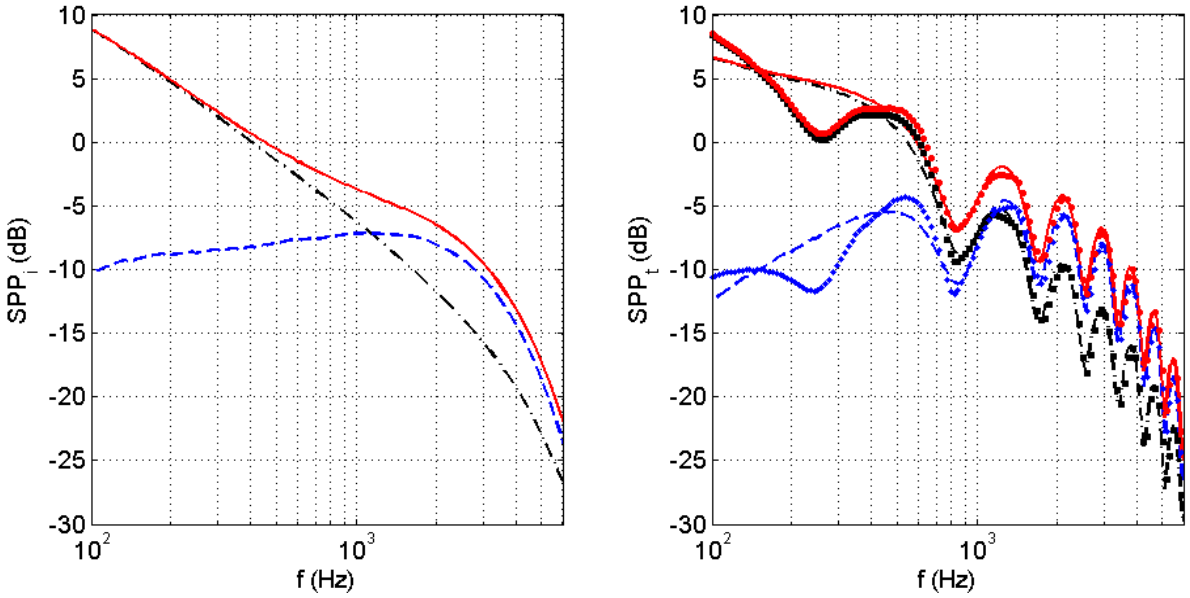

Figure 6: Incident (left) and total (right) acoustic PSD of the stationary airfoil: trailing-edge (blue dash), leading-edge (black dash-dot) ant total (solid red) with the analytical solution (curves) and ATV solution (symbols).

In presence of the scattering screen, accounting for the Equation (5) and superimposing two broadband noise sources, the total acoustic spectra can be obtained as shown in (right). Similarly, black, blue and red stand for leading-edge, trailing-edge and total acoustic spectra. The lines represent the scattering by an infinite screen obtaining via method of image sources where the exact solution obtained by means of ATV is shown in symbols. The total acoustic spectra accounting both leading- and trailing-edge contribution is again obtained via superimposing both scattered-field spectra of different noise models. Different than the incident field spectra, interference lobes appear due to the scattering of the acoustic field by the screen. A very good agreement is observed in comparison with the image source and ATV solution for high frequencies, validating the accuracy of the employed methodology. The additional oscillations at low frequencies are due to the scattering of the acoustic field by the finite-edges of the screen, which is neglected in the method of image sources. Since the ATV methodology is based on a BEM framework, it capable of handle finite and arbitrary geometries.

Once validated for a stationary observer, the methodology is later extended for a low-speed fan application. At rotational frequencies much lower than the acoustic frequencies of interest, $\boldsymbol{\omega} \gg \boldsymbol{\Omega}$, the circular motion can be approximated by locally tangential translation motion [18].

The Doppler Effect, which is due to the relative motion between the source and the observer, was shown to be negligible and the observed frequency converges to the emitted frequency [19]. In the current application the Mach number is 0.035 hence the Doppler effect is found to be negligible. The incident field PSD of a low Mach number axial fan with B blades is then computed with the integration on the azimuthal positions of the blade ψ as,

$$Spp_i(X,Y,Z,\omega) \cong \frac{B}{2\pi}\int_0^{2\pi} {Spp_i}^{\psi}(x,y,z,\omega)d\psi \tag{6}$$

assuming decorrelated source fields between the different blades [18]. This equation can also be applied for the scattered field problem by replacing ${Spp_i}^{\psi}(x,y,z,\omega)$ by ${Spp_t}^{\psi}(x,y,z,\omega)$ [6].

The methodology is applied to a generic low-speed axial fan with 4 blades. The blades are assumed to be flat plates for the sake of consistency with the previous CFD simulations. The chord and span-lengths are 0.04 m and 0.20 m, equal to the ones used in the airfoil predictions. The distance between the center of rotation and the center of the blade is equal to 0.12 m as sketched in Figure 5 (right). The rotational speed is selected equal to 1000 RPM, hence the same mean-flow velocity will impinge on the blade. The segmentation procedure detailed in references [9] is not employed, and the flow is assumed to be uniform in spanwise direction. The same scattering screen is introduced by the generic fan as shown in Figure 5 (right).

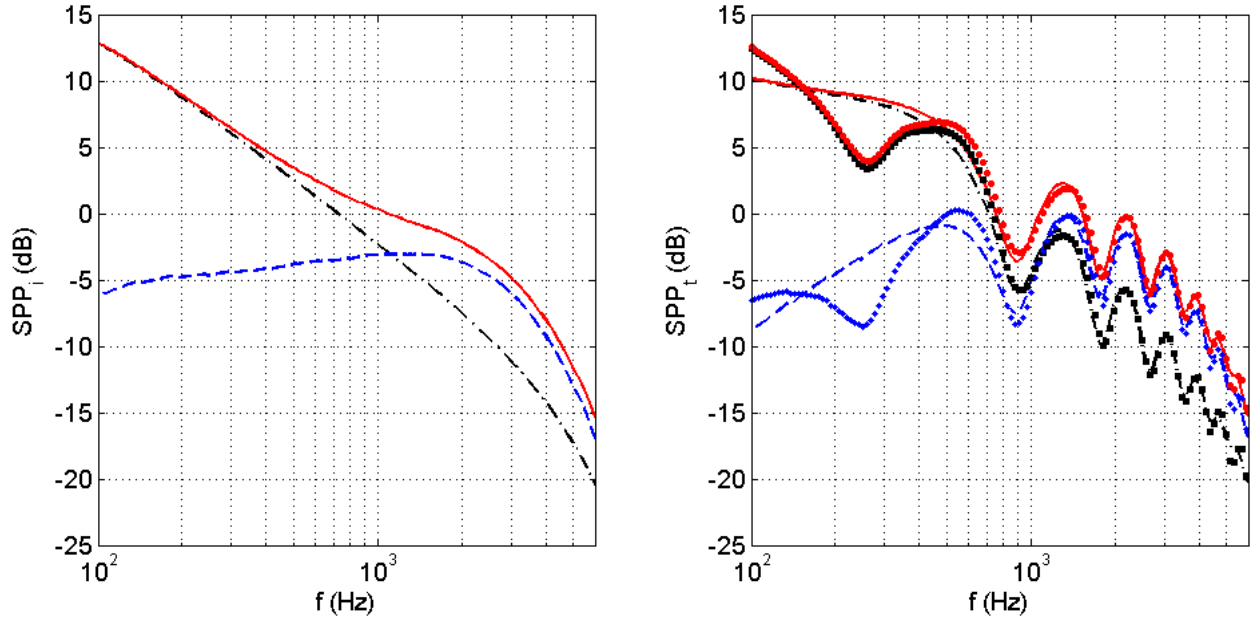

Figure 7: Incident (left) and total (right) acoustic PSD of the generic low-speed fan: trailing-edge (blue dash), leading-edge (black dash-dot) ant total (solid red) with the analytical solution (curves) and ATV solution (symbols).

Figure 7 (left) shows the acoustic incident field results of the low-speed axial fan. Similar to the ones in Figure 6 (left), the leading-edge and trailing-edge PSDs are shown in blue dash and black dash-dots. The total PSD is shown in red solid curve. It is seen that, for the given flow-field around the fan blades, the leading-edge noise is dominating the low-frequencies where the high frequency PSD are mostly due to the trailing edge contribution. The acoustic spectra of the fan and airfoil are observed to be similar, which is expected since the same turbulent flow parameters are employed. The azimuthal integration applied to represent the rotation of the fan only scales the acoustic field of the stationary airfoil. It is worth to note that the generic fan is a test-case of continuity with the flat-plate in order to validate the implementation of rotation prior to the application to more realistic cases.

Introducing the similar scattering screen, the total PSD of the fan is obtained using the ATV analogy is shown in Figure 7 (right). The blue, black and red represent trailing-edge, leading-edge and total acoustic PSD. The lines and symbols stand for method of image sources and the ATV solution. The total acoustic field is again fluctuating around the incident field SPD. A very good agreement is observed for the ATV solution in comparison with the analytical solution. The difference at low-frequencies is again due to the scattering of the acoustic waves by the free-edges of the obstacle, which are neglected in the analytical model. A more detailed presentation of the interference fringes is shown in Figure 8 for the stationary airfoil and generic low-speed fan applications. It can be seen that the ATV methodology is able to capture the interference lobes accurately for frequencies higher than 800 Hz for both stationary airfoil and the generic axial-fan. For frequencies below 800 Hz, the difference is due to the effect of the finite length of the scattering obstacle which is also taken into account into in the ATV solution.

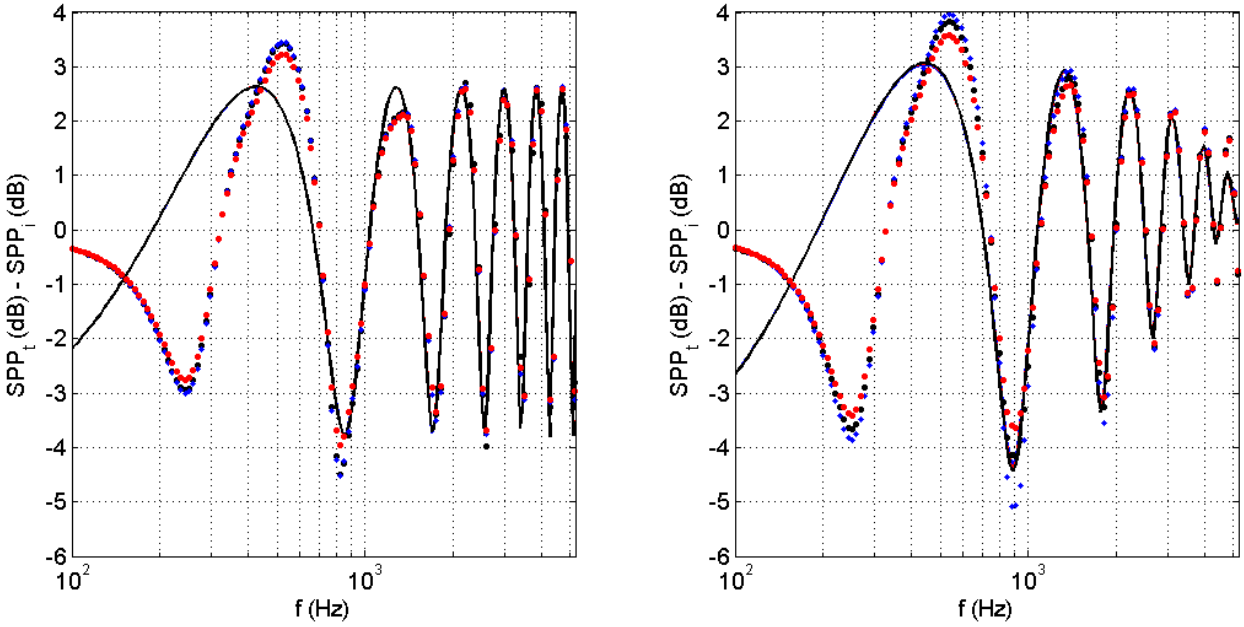

Figure 8: Interference fringes due to the scattering for the stationary airfoil (left) and generic axial fan (right): Analytical solution (curve) and ATV solution (symbols).

CONCLUSIONS

Both incident leading-edge and trailing-edge noise of a stationary airfoil have been first investigated in free-field. A flat plate with zero thickness exposed to different flow-fields with various turbulence parameters has been studied. In the first part of the paper, selection of a flow-field which generates different dominant broadband noise sources for different parts of the frequency spectrum has been focused. The outcome of the CFD simulations has been used as inputs in Amiet's semi-analytical theories for both leading-edge and trailing edge noise. The effect of different turbulence parameters such as turbulence intensity and length-scale on the acoustic PSD has been compared. Based on the assumption of uncorrelated mechanisms, the total acoustic response of the airfoil has been obtained. It has been showed that for the selected configuration, especially for high frequencies, both broadband noise mechanisms must be considered for a more accurate prediction.

Once the turbulence and flow parameters are set, the semi-analytical models have been extended for predictions in presence of scattering obstacles. The ATV methodology has been employed for the scattering predictions. The incident and scattered-field PSD have been computed using a geometrical near-field correction since the observer and scattering surface are located in the vicinity of the airfoil. A very good agreement has been obtained for the prediction of scattering of both leading-edge and trailing-edge noise models by a flat plate in comparison with the analytical solution which accounts for an infinite flat plate and an image airfoil.

The methodology has been later extended for a generic low-speed fan application. The rotation has been replaced by locally tangential translation motion. The same flow-field parameters have been used for the fan noise predictions. Implementing the ATV methodology and applying on scattering by a flat plate, a very good agreement has again been observed in comparison with the analytical solution which considers an infinite plate and an image fan. Since the ATVs are based on BEM framework, the proposed approach is capable of handling scattering by arbitrary geometries for both leading-edge and trailing-edge noise models and their combination.

ACKNOWLEDGEMENT

The authors are grateful to the EC for its support, provided in the framework of the FP7 Collaborative Project IDEALVENT (Grant Agreement no 314066). The support provided by the EC FP7 Initial Training Network FLOWAIRS (Grant Agreement no 289352) is thankfully acknowledged as well.

REFERENCES

[1] Moreau, S. and Roger, M. - Competing *Broadband Noise Mechanisms in Low-Speed Axial Fans*. AIAA Journal, 45(1), 48-57, **2007**.
[2] Caro, S., and Moreau, S. - *Aeroacoustic Modeling of Low Pressure Axial Flow Fans*. AIAA Paper 2000-2094, **July 2000**.
[3] Wright, S. E. - *Acoustic Spectrum of Axial Flow Machines*. Journal of Sound and Vibration, Vol. 45, No. 2, pp. 165–223, **1976**.
[4] Amiet, R. K. - Acoustic *Radiation from an Airfoil in a Turbulent Stream*. Journal of Sound and Vibration, 41, 407-420, **1975**.
[5] Amiet, R. K. - *Noise due to Turbulent Flow past a Trailing Edge*. Journal of Sound and Vibration, 47, 387-393, **1976**.
[6] *Virtual.Lab Rev 13: User Manual*, LMS International, **2013**.
[7] Bailly, C., Juve, D. - *Numerical Solution of Acoustic Propagation Problems Using Linearized Euler Equations*. AIAA Journal 38 (1): 22-29, **2002**.
[8] Seongkyu L., Kenneth S. B., and Philip J. M. - *Acoustic Scattering in the Time Domain Using an Equivalent Source Method*. AIAA Journal, Vol. 48, No. 12, 2772-2780, **2010**.
[9] Kucukcoskun, K., Christophe, J., Schram, C. and Tournour, M. - *Broadband scattering of the turbulence interaction noise of a stationary airfoil: experimental validation of a semi-analytical mode.* International Journal of Aeroacoustics, 12, 85 – 104, **2013.**
[10] Gerard, F., Tournour, M., Masri, N.E., Cremers, L., Felice, M., Selmane, A. - *Numerical Modeling of Engine Noise Radiation Through the Use of Acoustic Transfer Vectors: A Case Study*. SAE Paper, 2001-01-1514, **2001**.
[11] Roger, M. and Moreau, S. - *Back-Scattering Correction and Further Extensions of Amiet's Trailing-Edge Noise Model. Part 1: Theory*. Journal of Sound and Vibration, 286, 477-506, **2005**.
[12] Moreau, S.; Roger, M. and Jurdic, V. - *Effect of Angle of Attack and Airfoil Shape on Turbulence-Interaction Noise*. 11th AIAA/CEAS Aeroacoustics Conference, **2005**.
[13] Kucukcoskun, K., Christophe, J., Schram, C. and Tournour, M. - *Free and scattered acoustic field predictions of the broadband noise generated by a low-speed axial fan*. Noise Control Engr. J. 61 (2), **2013**.
[14] Denayer, H., De Roeck, W., Desmet, W. and Schram, C. - *Extension of Amiet's Theory for the Aeroacoustic Analysis of a Wing-Flap Configuration Including Acoustic Scattering*. 18th AIAA/CEAS Aeroacoustics Conference (33rd AIAA Aeroacoustics Conference), 10.2514/6.2012-2096, **2012.**
[15] Panton, R. L. and Linebarger, J. H. - *Wall Pressure Spectra Calculations for Equilibrium Boundary Layers.* J. Fluid Mech., Cambridge Univ Press, 65(2), 261-287, **1974**.
[16] Remmler, S.; Christophe, J.; Anthoine, J. and Moreau, S. - *Computation of Wall-Pressure Spectra from Steady Flow Data for Noise Prediction*. AIAA Journal, 48(9), 1997-2007, **2010**.
[17] Corcos, G. M. - *The structure of the turbulent pressure field in boundary-layer flows*. Journal of Fluid Mechanics, 18(3), 353–379, **1964**.
[18] Paterson, R.W. and Amiet, R.K. - *Noise of a Model Helicopter Rotor due to Ingestion of Turbulence*. NASA, TR-CR 3213, **1979**.
[19] Morfey, C.L. and Tanna, H.K. - *Sound radiation from a point force in circular motion.* J. Sound Vibr., 15(3), 325–351, **1971**.